Supplemental Information

Bioinformatic and biochemical analysis uncovers novel activity in the 2-ER Subfamily of OYEs

Tamra C. Blue, Stacey K. Jones, and Katherine M. Davis*

Department of Chemistry, Emory University, Atlanta, Georgia 30322, United States

Table of Contents

Table S1. Domains identified in 2-ERs across all numbered clusters. FAD-dependent domains are highlighted in red.

No.	Pfam	Domain	# nodes	% prevalence
D1	PF00724	FMN-binding	5744	100
D2	PF00070 (PF07992)	Pyridine nucleotide-disulphide oxidoreductase (NADH-binding domain within FAD-binding domain)	5073 (15)	89
D3	PF13450	FAD/NAD(P)-binding oxidoreductases	345	6
D4	PF12831 (PF01266)	FAD-dependent oxidoreductases	87 (2)	1.5
D5	PF03486	HI0933-like protein	29	0.5
D6	PF00070	Pyridine nucleotide-disulphide oxidoreductase	15	0.26
D7	PF06314	Acetoacetate decarboxylase	14	0.24
D8	PF00890 (PF01494)	FAD-binding	9 (2)	0.2
D9	PF00378	Enoyl-CoA hydratase/isomerase	8	0.14
D10	PF01370	NAD dependent epimerase/dehydratase family	7	0.12
D11	PF10518	TAT pathway signal sequence	4	0.07
D12	PF12680	SnoaL-like domain	4	0.07
D13	PF01134	Glucose inhibited division protein A	3	0.05
D14	PF00582	Universal stress protein family	2	0.03
D15	PF00753	Metallo-beta-lactamase protein fold	1	0.02
D16	PF00787	PX domain	1	0.02
D17	PF08790	LYAR-type C2HC zinc finger	1	0.02
D18	PF07238	PilZ domain	1	0.02

Table S2. Substrate scope of OYE*Bi*. Biotransformations were conducted in a 100 mM phosphate buffer, pH 8, supplemented with NADH.

	Anaerobic	**Pseudo-Anaerobic (reconstituted)**	**Aerobic (reconstituted)**
1→2	100%	61.88±2.12% (73.41±12.25%)	6.52±4.17 (7.93±3.26%)
2→1	n.d.	n.d.	n.d.
3→3P	10.80±0.50%	0.26±0.02% (0.54±0.01%)	0.33±0.03% (n.d.)
4→4P	n.d.	n.d. (0.32±0.01%)	n.d.
5→5P	2.12±0.26%	2.11±0.04% (1.82±0.22%)	0.21±0.01 (n.d.)
6→6P	1.50±0.42%	n.d.	n.d.
7→7P	n.d.	n.d.	n.d.
8→8P	n.d.	n.d.	n.d.
9→9P	22.16±2.24%	8.59±0.20% (13.66±0.32%)	1.94±0.12% (0.10±0.04%)
10→9	1.50±0.12%	n.d. (0.63±0.01%)	7.06±0.38% (2.31±0.22%)
10→9P	2.29%±1.18%	0.37±0.10% (0.47±0.00)%	0.32±0.42% (n.d.)

Table S3. Genomic neighborhood analysis.

Pfam accession #	Description	CoF
PF01012	Electron transfer flavoprotein domain (ETF)	41%
PF00766-PF01012	Electron transfer flavoprotein FAD-binding domain fused to an electron transfer flavoprotein domain (ETF_alpha-ETF)	41%
PF00355-PF00848	a Rieske [2Fe-2S] domain fused to a ring hydroxylating alpha subunit catalytic domain (Rieske-Ring_hydroxyl_A)	40%
PF00111-PF00175-PF00970	2Fe-2S cluster binding domain fused to an oxidoreductase NAD-binding domain and an oxidoreductase FAD-binding domain	38%
PF19367	Domain of unknown function (DUF)	36%
PF00126-PF03466	bacterial regulatory helix-turn-helix protein of the lysR family fused to a lysR substrate binding domain (HTH_1-LysR_substrate)	36%
PF01244	Membrane dipeptidase (Peptidase family M19)	36%
PF01965-PF12833	Domain of the DJ-1/PfpI family fused to a helix-turn-helix domain (DJ-1_PfpI-HTH_18)	35%
PF04069	Substrate binding domain of a ABC-type glycine betaine transport system (OpuAC)	34%
PF00528	Binding protein dependent transport system inner membrane component (BPD_transp_1)	27%
PF00440	Bacterial regulatory proteins of the tetR family (TetR_N)	24%
PF00005	ABC transporter (ABC_tran)	21%
PF00107-PF08240	Zn-binding dehydrogenase domain fused to an alcohol dehydrogenase GroES-like domain (ADH_zinc_N-ADH_N)	20%

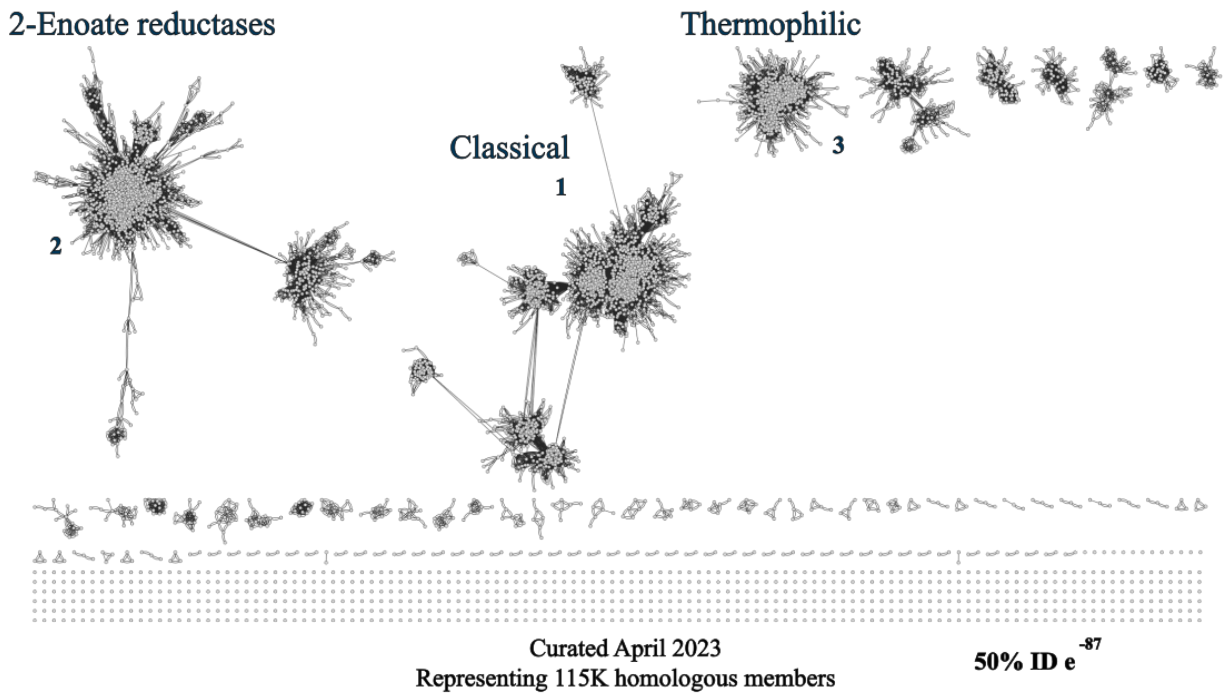

Figure S1. SSN of OYE family (PF00724).

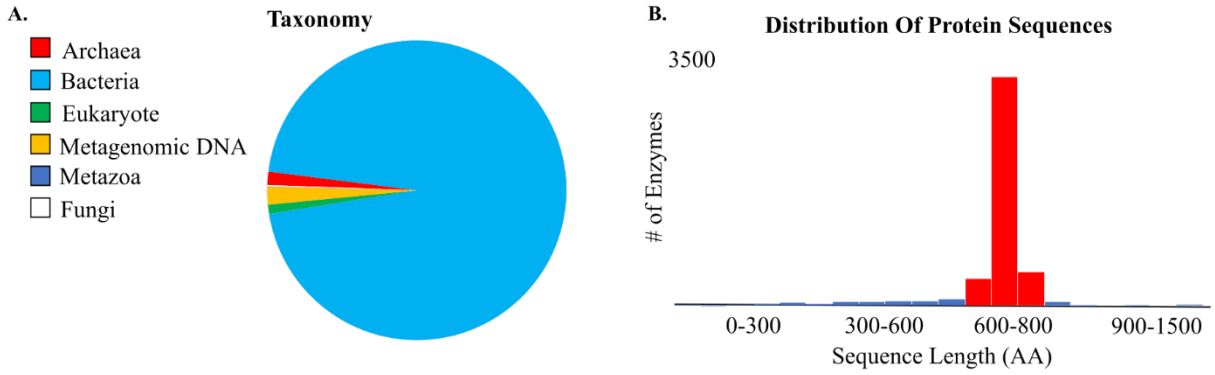

Figure S2. (A) Taxonomy and (B) average length of sequences of 2-ERs within the OYE family.

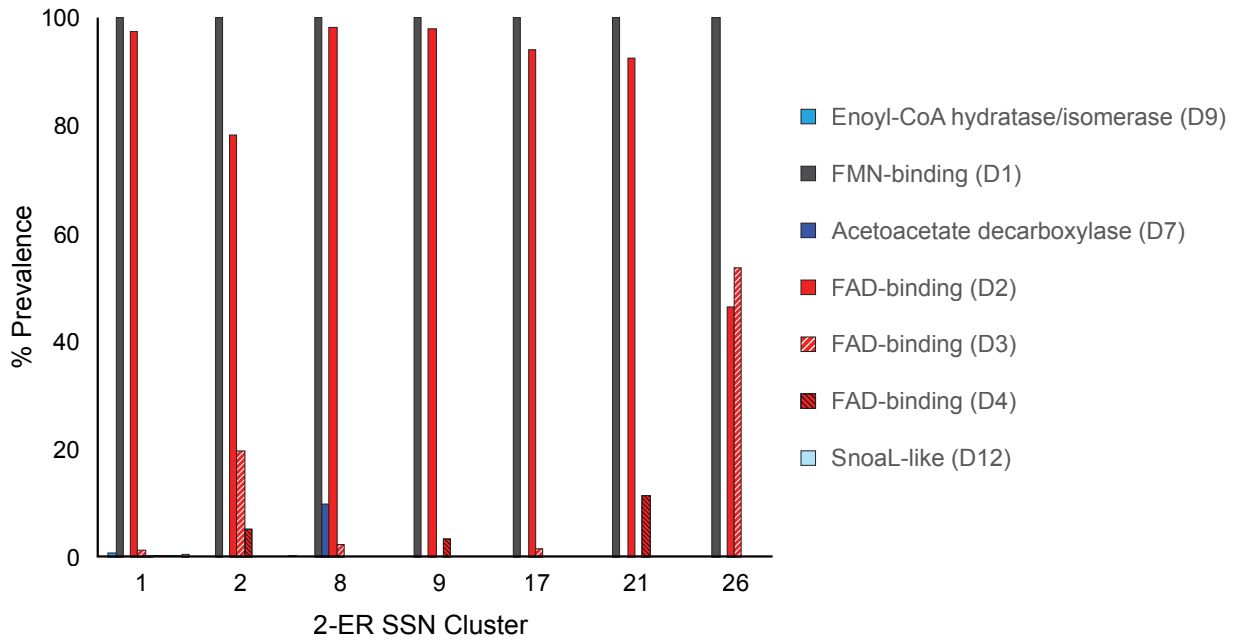

Figure S3. Prevalence of Pfam domains by 2-ER SSN cluster. Cluster 1 serves as the canonical 2-ER control. OYE*Bi* is from cluster 2. Clusters 8, 9, 17, 21, and 26 lack the Fe/S cluster-binding motif. Domain numbering is according to Table S1. Note that domains with prevalence <0.25% are not visible in this chart.

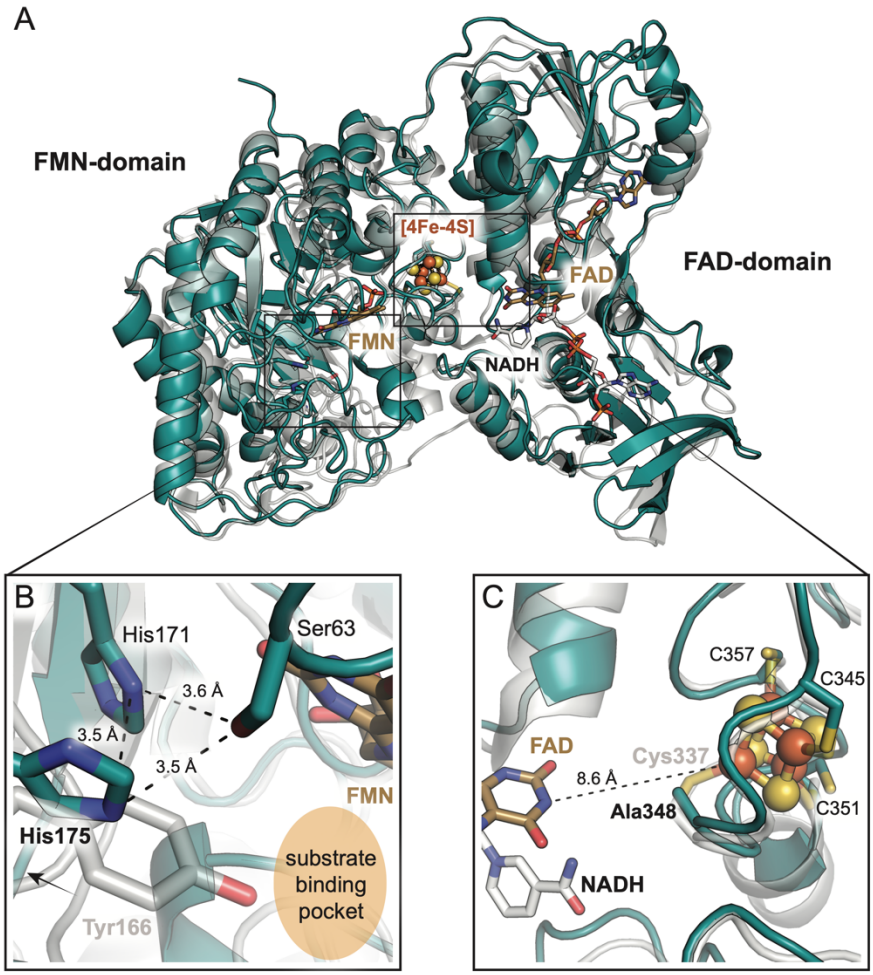

Figure S4. Alignment of the OYE*Bi* AlphaFold model (teal) and the crystal structure of DCR (PDB accession code 1PS9; grey). Comparison of their (A) global structures, (B) active sites, and (C) Fe/S cluster-binding motifs.

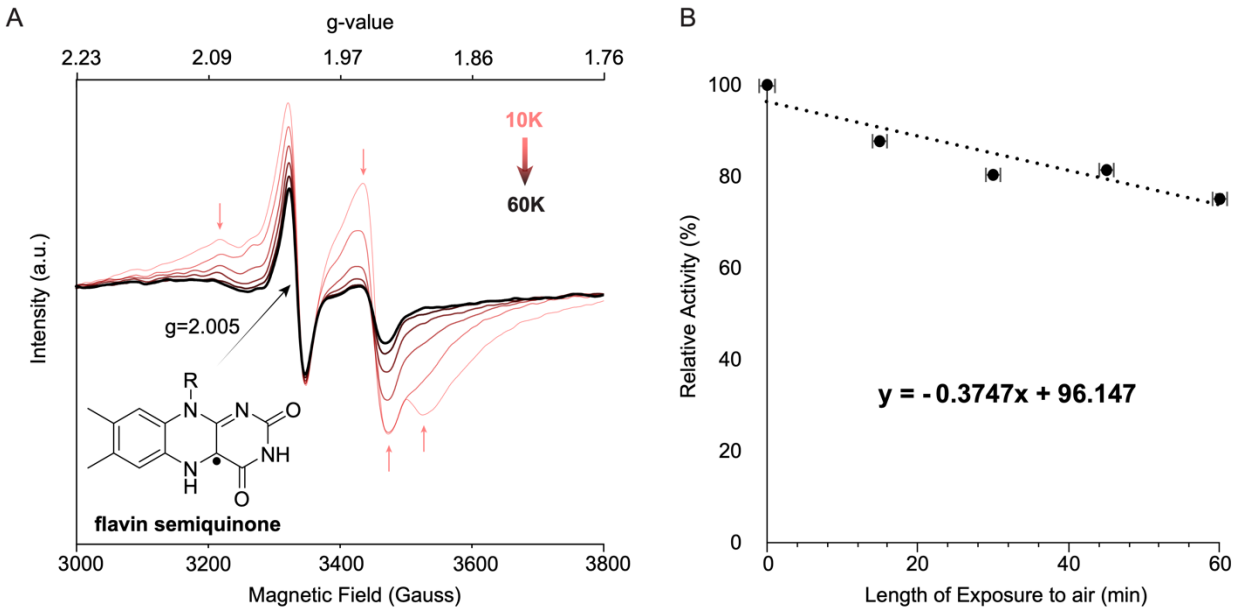

Figure S5. (A) X-band EPR spectra with increasing temperature depicts convergence to flavin radical signal upon loss of the rhombic features associated with the [4Fe-4S] cluster. (B) Reduction in activity upon exposure to oxygen assessed by GC-MS.

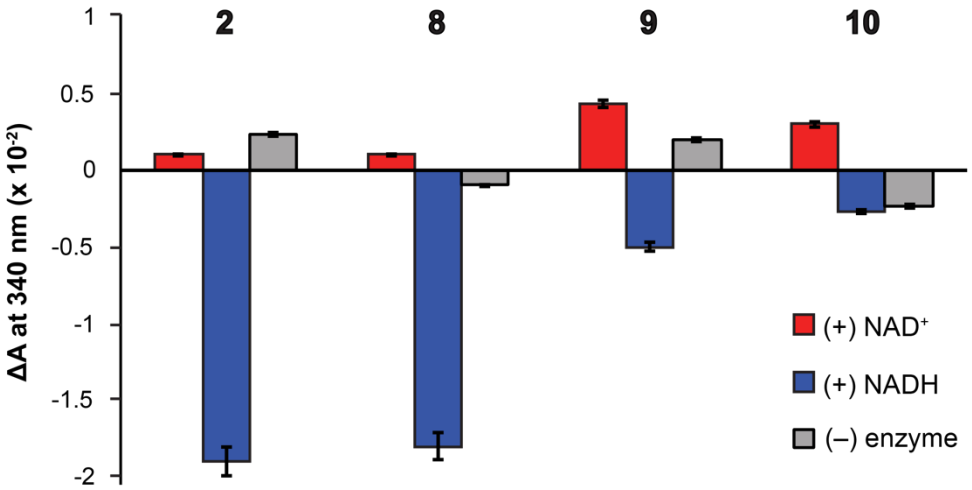

Figure S6. Assessment of NAD^+ dependent activity. NADH production (red) or consumption (blue) by OYE*Bi* in the presence of substrates probing oxidation activity were assessed by the change in absorbance at 340 nm. Assays conducted in the absence of glucose dehydrogenase and glucose revealed no detectable conversion of NAD^+ to NADH for either demethylation or desaturase activity. A no enzyme control was also performed in the absence of enzyme and nicotinamide cofactor.

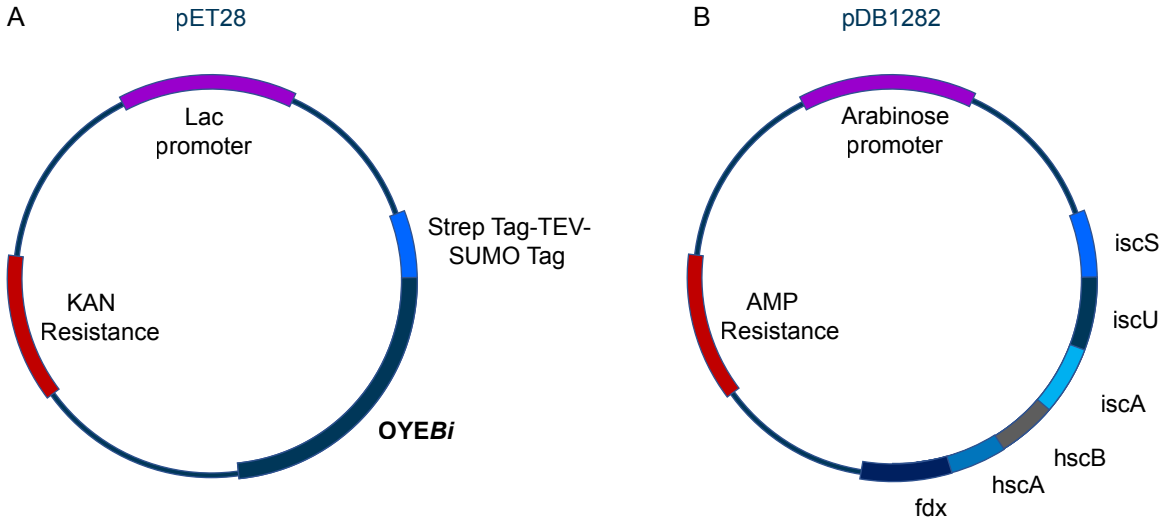

Figure S7. Cartoon representations of the (A) pET28 vector encoding OYE*Bi* and (B) pDB1282 vector encoding the *isc* operon.